EUROfusion

WPDTT1-CPR(18) 20064

M Poradzinski et al.

Integrated Power Exhaust Modelling for DEMO with Lithium Divertor

Preprint of Paper to be submitted for publication in Proceeding of
30th Symposium on Fusion Technology (SOFT)

This work has been carried out within the framework of the EUROfusion Consortium and has received funding from the Euratom research and training programme 2014-2018 under grant agreement No 633053. The views and opinions expressed herein do not necessarily reflect those of the European Commission.

Integrated power exhaust modelling for DEMO with lithium divertor

M. Poradziński, I. Ivanova-Stanik, G. Pełka, V. Pericoli Ridolfini, R. Zagórski

Institute of Plasma Physics and Laser Microfusion, Hery str. 23, 01-497, Warsaw, Poland

Abstract

A DEMO reactor with a liquid lithium divertor setup is considered. The simulation is performed for EU DEMO 2018 configuration using COREDIV code which self-consistently solves core and scrape-off layer transport equations for plasma and impurity. Influence of the sputtering, prompt redeposition and evaporation of the liquid lithium divertor was taken into account. Two operation regimes were identified. In the first regime evaporation rate is suppressed by the cooling system and is of the order of the sputtering rate. Scrape-off layer plasma characterises with low radiation and high total power to the plates. In the second regime cooling is less effective and evaporation is much higher than the sputtering rate. High Li influx reduces temperature in the divertor region. Lithium radiation is increased reducing power to the plates. Plasma parameters in the core are comparable for the two regimes. Both regimes characterise with high plasma dilution. Power across the separatrix stays above the L-H threshold.

Keywords: DEMO, Liquid Metal Divertor, impurity, lithium, numerical modelling

1. Introduction

Operation of a future demonstration fusion reactor (DEMO) requires handling of a significant power flux across the separatrix. A considerable amount of energy has to be dissipated before the heat flux reaches the divertor plates. The divertor may be exposed to high heat fluxes causing high temperature gradients and material fatigue. Such challenging conditions in the scrape-off layer (SOL) demands developing solid state plate protection scenarios. In the liquid metal divertor [1], which is one of the considered solutions to the power exhaust problem, a liquid surface protects the solid plates against high heat loads, allowing for longer operation without the need of the divertor disassembly.

Self-replenishing liquid surfaces would eliminate some issues such as melting and re-crystallization that could degrade solid PFCs [2]. A liquid metal (LM) divertor can be realized via capillary porous system (CPS) which consists of a mesh or a porous structure in which liquid metal flows. A CPS considered in a LM divertor stabilizes the surface and suppresses withdrawing the liquid metal droplets to the SOL region by $j \times B$ forces. A CPS scheme for a liquid divertor has proven to be the most promising configuration to confine liquid metal against MHD effects, by means of capillary forces [3, 4].

Liquid lithium (Li, Z=3) is one of the promising candidates for LM divertor due to its low melting point and high vapor pressure [5] (see Tab. 1). There are two sources of lithium in plasma, sputtering and evaporation. Low Li threshold energy for D and T sputtering (see Fig. 1.) leads to high Li impurity content in the SOL. Contrary to the sputtering, evaporation rate can be controlled by means of the cooling system [6]. Lithium radiation in the SOL depends on the electron density and temperature in the edge (see Fig. 2). High temperature in the SOL prevents Li radiation, energy is not dissipated what results in high target power load in spite of relatively high plasma dilution by lithium ions.

In this paper we analyse a liquid lithium divertor target

	W	Li
Atomic number	74	3
Melting point, °C	3422	180.5
Boiling point, °C	5930	1330
Thermal conductivity at 800 K, W/m/K	127.0	54.4
Heat of evaporation, kJ/mol	806.7	136

Table 1: Lithium and tungsten physical properties.

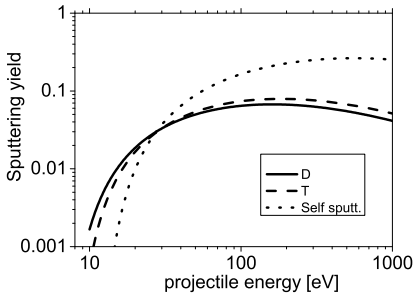

Figure 1: Sputtering yield for lithium target at normal incident angle.

Email address: michal.poradzinski@ipplm.pl
(M. Poradziński)

power load dependence on lithium particle influx to the plasma. A possible operational space for EU DEMO 2018 scenario with lithium divertor setup is found. Influence of the sputtering, prompt redeposition and evaporation of the liquid Li divertor is taken into account. Modelling approach is described in Section 2. Results and discussion are presented in section 3.

2. Modelling approach

Energy balance in tokamaks with metallic walls depends strongly on the coupling between the bulk and the scrape-off layer (SOL) plasma, modelling requires the transport problem to be addressed in both regions simultaneously. The above statement applies also to a scenario with a liquid lithium divertor. Although lithium is not expected to radiate siginificantly in the core (see Fig. 2.), it affects core performance by diluting plasma and therefore reducing the fusion power. As a result reduced by dilution but still high power flux across the separatrix affects the edge plasma and the divertor conditions.

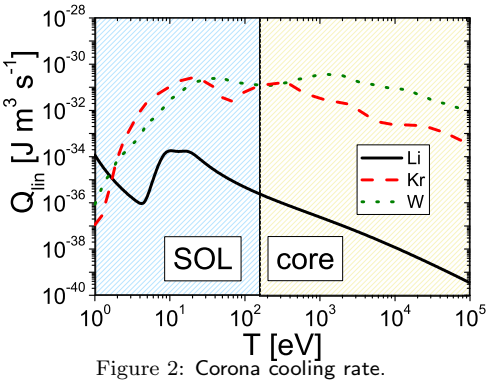

Figure 2: Corona cooling rate.

2.1. COREDIV

Simulations were performed with the COREDIV code [7] which self-consistently solves 1D radial transport equations of plasma and impurities in the core region and 2D multi-fluid transport based on Braginskii-like equations in the scrape-off layer region. The code has been successfully benchmarked with a number of JET ILW discharges, including the nitrogen and neon seeded [8, 9]. COREDIV has also been applied to ASDEX discharges in the full W environment [10]. The physics model used in the COREDIV code is relatively complex and has been already presented elsewhere [7, 8, 11, 12]. Transport model in the core used in this simulation is described in Ref. [13]. The SOL region is approximated by a simple slab geometry (poloidal and radial direction) with classical transport in the poloidal direction and anomalous transport in the radial direction. Similarly as, in the core part of the model, it is assumed that for all ions the anomalous transport is the same and they have the same temperature. We used for the value of radial anomalous transport in the SOL $D_{rad}^{SOL} = 0.42\mathrm{m}^2/\mathrm{s}$. Thermal conductivities are set to $\chi_{e,i} = 0.18\mathrm{m}^2/\mathrm{s}$. Values for D_{rad}^{SOL} and $\chi_{e,i}$ are chosen to be the same as in TECXY simulations for DEMO with liquid metal divertor [14] in order to facilitate further comparison studies. Tritium production from neutron-lithium collisions is not included in the model.

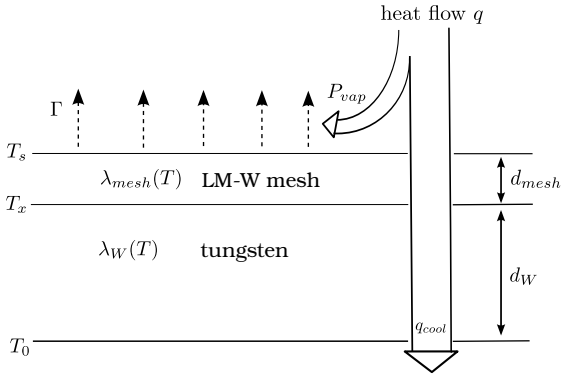

Figure 3: Liquid metal divertor scheme.

2.2. Lithium evaporation model

Sputtering of D, T, He, self sputtering of Li on Li target and evaporation of Li impurity add up to the total Li impurity influx to the plasma. Evaporation model implemented in COREDIV code was first presented for tin in Ref. [13]. Tin boiling point is much higher than lithium one (see Table 1). For this reason, lithium evaporation modelling requires including enthalpy of evaporation.

A one dimensional LM divertor scheme is presented in Fig. 3. Heat flux q is an input of the model and evapoartion rate Γ is an output. Parameters d_{mesh} and d_W are a liquid metal mesh layer and a tungsten layer thicknesses respectively. Lithium and tungsten thermal conductivities $\lambda_i(T)$, i= Li, W for reference values at 800°K are given in Table 1. Liquid metal mesh thermal conductivity is an average of tungsten and lithium thermal conductivities. Coolant temperature T_0 is a parameter of the model and is kept constant during simulation. Heat flux q is split into the heat flux q_{cool} which is transferred without losses further to the bottom of the divertor plate and into latent heat of evaporation P_{vap},

$$q = q_{cool} + P_{vap}. \quad (1)$$

Latent heat of evaporation is proportional to the evaporation rate Γ, $P_{vap} = h_{vap}\,\Gamma_{vap}$, where the coefficient h_{vap} is a latent heat of evaporation per one particle. Temperatures T_x and T_s are the tungsten-mesh contact surface temperature and the LM surface temperature, respectively. A flux of particles $\Gamma\,[\mathrm{m}^{-2}\mathrm{s}^{-1}]$ leaving the divertor surface is given by the Hertz-Knudsen equation.

2.3. Influence of T_0 and d_W on evaporation rate

Influence of the coolant temperature T_0 and tungsten layer thickness on the evaporation is shown in Fig. 4. In-

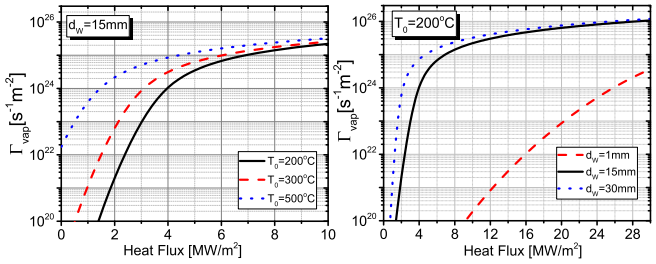

Figure 4: Evaporation rates as a function of local heat flux to the plate for $d_{\text{mesh}} = 1\text{mm}$.

creasing coolant temperature reduces cooling effectiveness and high evaporation rates are expected at lower heat flux values. We observe that evaporation rate reaches $\Gamma_{vap} = 10^{24} s^{-1} m^{-2}$ at $q = 1.5\text{MW/m}^2$ in the case of $T_0 = 500°\text{C}$. At $T_0 = 200°\text{C}$, the same evaporation rate level is reached for $q \simeq 4\text{MW/m}^2$. Increase of the W layer width leads to a strong reduction of the critical heat flux. In the case of $d_W = 30\text{mm}$ evaporation rate of the size of $10^{24}\,\text{m}^{-2}\text{s}^{-1}$ is reached at the local heat flux level of $2\,\text{MW/m}^2$ whereas in the case of $d_W = 1\text{mm}$ the evaporation rate is strongly suppressed and requires heat flux of the order of $25\,\text{MW/m}^2$ to reach the $10^{24}\,\text{m}^{-2}\text{s}^{-1}$ value.

3. Simulation of liquid lithium divertor

Simulations were performed according to the EU DEMO 2018 configuration computed by means of PROCESS [15] with the following main parameters: toroidal radius $R_T = 9.002\text{m}$, minor plasma radius $a = 2.904\text{m}$, plasma current $I_p = 17.75\text{MA}$, toroidal magnetic field $B_T = 5.855\text{T}$, elongation $\varepsilon = 1.65$, volume averaged electron density $\langle n_e \rangle_{\text{VOL}} = 7.261 \times 10^{19}\text{m}^{-3}$, L-H transition power threshold $P_{LH} = 120.8\text{MW}$, H-factor (IPB98(y,2)) $H98 = 1.1$ and auxiliary heating power P_{aux} equal to 50MW. Throughout the simulation the temperature $T_0 = 200°\text{C}$ was used.

3.1. Influence of the angle α_{div}

Implementing the evaporation model into COREDIV code required introducing a new parameter which is the angle (α_{div}) between magnetic field line and divertor plate. In order to assess how the angle α_{div} affects the evaporation rate a scan was performed for α_{div} ranging from 1° to 6°. For comparison, a second scan was performed for d_W ranging from 1mm to 30mm.

Evaporation rate and total sputtering dependence on α_{div} and d_W are presented in Figure 5. Total sputtering weakly depends on α_{div} and d_W changing from $2.2 \times 10^{23} s^{-1}$ to $3.0 \times 10^{23} s^{-1}$. Evaporation rate increases with both α_{div} and d_W ranging from $6.5 \times 10^{23} s^{-1}$ up to $2.75 \times 10^{24} s^{-1}$.

Total Li influx (Γ_{Li}) is a monotonic function of both α_{div} and d_W. Results of the d_W scan were used in further analysis and the angle α_{div} was set to 3° throughout the simulation.

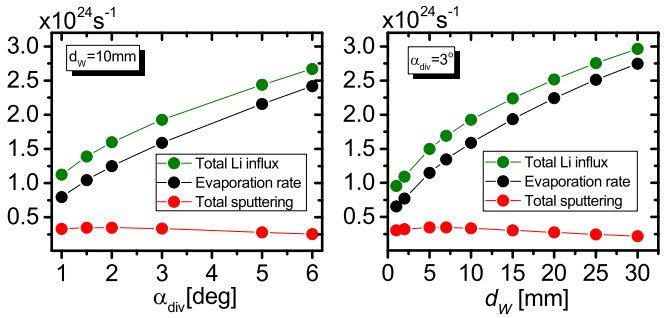

Figure 5: Total Li influx, Lithium evaporation and sputtering dependence on the angle α_{div} and on tungsten layer depth d_W for $n_{sep} = 2.9 \times 10^{19}\text{m}^{-3}$.

3.2. Influence of the density at the separatrix

Total Li influx (Γ_{Li}) and Li concentration in the core as a function of the density at the separatrix are presented in Figure 6. Increasing density at the separatrix leads to the higher Li concentration in the core and simultaneously decreases the lithium influx Γ_{Li}. Lithium concentration reaches a maximum value of 15.7% for $n_{sep} = 4.1 \times 10^{19}\text{m}^{-3}$ what corresponds to 56.5% of $\langle n_e \rangle_{\text{VOL}}$. Maximum local power to plate (P^{max}_{plate}) and the electron to ion density ratio at the plate dependence on d_W in the case of low and high density at the separatrix are presented in Figure 7. Maximum local power to the plate drops down to 5MW/m^2 with tungsten substrate width. Since evaporation is a steep function of the heat flux density (see Fig. 4), solution is to be found in narrow range of possible heat flux values for given divertor settings. Therefore, maximum local power to the plate is determined by the divertor settings and does not depend on the density at the

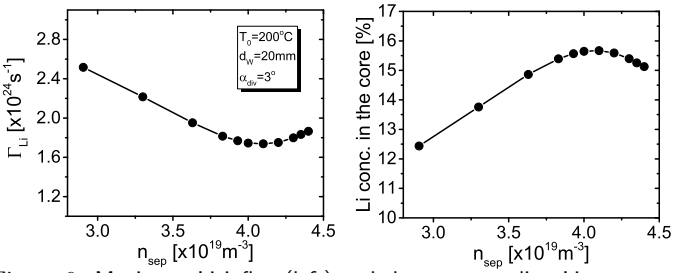

Figure 6: Maximum Li influx (left) and the corresponding Li concentration in the core (right) dependence on density at the separatrix.

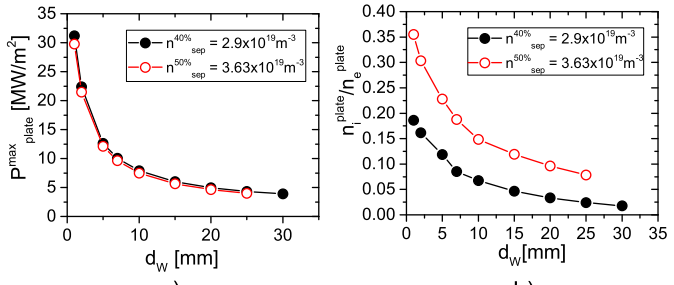

Figure 7: a) Maximum local power to the plate P^{max}_{plate}, and b) electron to ion density ration at the plate dependence on lithium influx Γ_{Li}.

separatrix. COREDIV is a self-consistent core-SOL code. Solution is found by adjusting fusion power P_α, radiation in the core and radiation in the SOL to match the imposed power to the plate.

The ratio $n_i^{plate}/n_e^{plate} = 0.19$ (low density at the separatrix) at $\Gamma_{Li} = 0.96 \times 10^{24}\mathrm{s}^{-1}$ whereas for high evaporation values $\Gamma_{Li} = 3 \times 10^{24}\mathrm{s}^{-1}$ is an order of magnitude lower $n_i^{plate}/n_e^{plate} = 0.018$. This is the result of high Li dilution in the divertor region.

Dependence of the main core and SOL parameters on the divertor substrate width is shown in Figure 8. The results are presented for $n_{sep}^{40\%} = 2.9 \times 10^{19}\mathrm{m}^{-3}$ (low density) and $n_{sep}^{50\%} = 3.63 \times 10^{19}\mathrm{m}^{-3}$ (high density). For both n_{sep} values total power to the plate (P_{plate}) drops down with d_W from the level of 150MW to the level of 40MW (Fig. 8 a)). Although P_{plate}^{max} does not depend on n_{sep}, one observes a difference between the values of P_{plate} for the two values of n_{sep}. This is attributed to the difference between the P_{plate} profiles at the plate. The electron temperature at the plate (T_e^{plate}) (Fig. 8b), decreases from 65eV down to values below 10eV. As in the case of the maximum power to the plate, the electron temperature at the plate practically does not depend on the density at the separatrix. The temperature decrease is accompanied by increase of Li radiation (Fig. 8 b) what is expected as lithium line radiation reaches a maximum plateau from about 8eV to 20eV (see Fig. 2.). Lithium radiation in the SOL reaches 155MW for low density at the separatrix but only 120MW for high density at the separatrix. This difference can be explained by the plasma conditions in the core. Lithium concentration in the core (Fig. 8c) is as high as 14.8% in the case of high density at the separatrix and 12.6% in the case of low density at the separatrix. Higher Li plasma dilution in the core reduces heating from the α particles and results in lower power across the separatrix (P_{SOL} in Fig. 8d). Power across the separatrix in the case of high density at the separatrix decreases to 164MW whereas in the case of low density at the separatrix it drops down to 203MW with d_W. This 20% difference accounts for the 20% difference in lithium radiation in the SOL between low density at the separatrix and high density at the separatrix. Difference in Li core dilution between the two considered values of the density at the separatrix also results in lower fusion gain Q in the case of high density at the separatrix. In the case of low density at the separatrix Q varies from 23 to 25 and at high density at the separatrix Q varies from 19 to 22 depending on the Li influx (see Fig. 8d). Since lithium radiates in the core only by means of bremstrahlung and synchrotron radiation, radiation in the core weakly depends on the Li influx and on the density at the separatrix. Its value remains at the level of 80MW (see Fig. 8c).

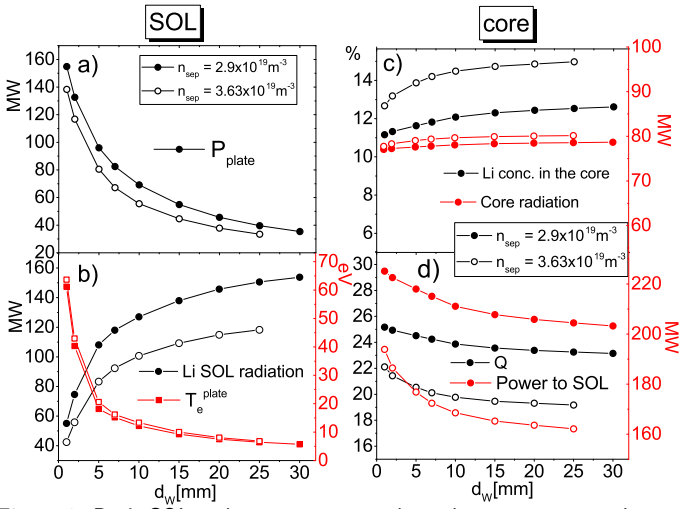

Figure 8: Basic SOL and core parameters dependence on tungsten layer width d_W.

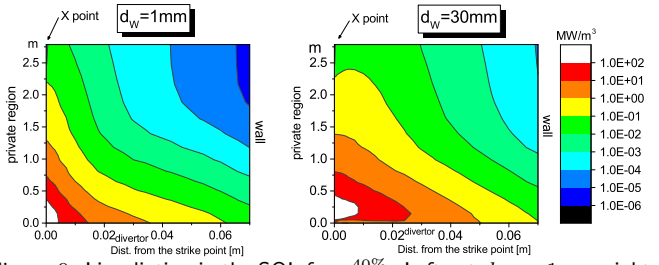

Figure 9: Li radiation in the SOL for $n_{sep}^{40\%}$. Left: at $d_W = 1$mm, right: at $d_W = 30$mm.

Two dimensional contour plots of lithium radiation in the divertor region for two values of the parameter d_W (1mm and 30mm) are presented in Figure 9. In the case of low cooling effectiveness ($d_W = 30$mm) Li radiation in the divertor region is broader across the plate and extends further towards the X point. The highest radiation region ($> 10\mathrm{MW/m}^3$) is detached from the divertor plate. A form of a vapor shield is created above the strike point.

Evap. regime	low		high	
$n_{sep}[\times 10^{19}m^{-3}]$	2.9	3.63	2.9	3.63
d_W[mm]	1	1	20	20
$\Gamma_{vap}[\times 10^{23}\mathrm{s}^{-1}]$	6.5	4.27	22.4	17.2
$\Gamma_{sputt}[\times 10^{23}\mathrm{s}^{-1}]$	3.0	2.8	2.74	2.3
P_{plate}[MW]	155	138	45.7	37.9
P_{plate}^{max}[MW/m^2]	31.2	29.8	5.0	4.6
T_{surf}^{max}[°C]	748	727	766	755
T_e^{plate}[eV]	61	64	7.5	8.1
f_{rad}[%]	50	50	85.4	86.6

Table 2: Plasma parameters in case of low and high evaporation regime for two values of densities at the separatrix. The angle $\alpha_{div} = 3°$.

Comparing presented results one can observe two regimes of operation. First regime corresponds to Li influx values below $1. \times 10^{24}\mathrm{s}^{-1}$ and second regime corresponds to Li influx values higher than $1.5 \times 10^{24}\mathrm{s}^{-1}$. Comparison of plasma and divertor plate parameters is presented in Table 2. In the first regime effective cooling suppresses

evaporation rate which is twice as high as the sputtering rate. In this regime total power to the plate reaches 160MW at low density at the separatrix and local maximum power to the plate is as high as 32MW/m^2. Second regime corresponds to the low cooling effectiveness (high tungsten layer width). Such conditions imply higher evaporation rate which is coupled with the local power to the plate. Higher evaporation rate reduces power to the plate by means of Li radiation in the divertor region. Reduction of the local power to the plate is followed by lower evaporation and a new equilibrium is established. High evaporation regime characterises with lower electron temperature at the plates ($<$ 10eV), lower total power to the plates ($<$ 40MW) and high lithium radiation in the SOL of the order of 150MW.
In both regimes conditions in the core stays almost the same. Lithium concentration in the core increases slightly and radiation in the core stays at the same level. Although the radiation fraction exceeds 85% in the high evaporation regime it is mostly due to high lithium radiation in the SOL. The power across the separatrix P_{SOL} is well above the L-H threshold which is 120.8MW according to the scaling laws [18, 15].

4. Conclusions

The self-consistent (core-edge) COREDIV code has been used to analyze DEMO with liquid lithium divertor. The core-SOL energy balance is found by adjusting fusion power, radiation in the core and in the SOL to match the power to the plate defined by the divertor settings. Two operation regimes were identified. They correspond to high and low evaporation rate compared to the sputtering rate. In the case when the evaporation rate is suppressed a low evaporation regime is established. It characterises with high divertor power load which can be explained by electron temperature at the plate as high as 160eV and relatively low Li dilution. In such conditions lithium radiation in the SOL stays at the level of $40-50$MW which is not enough to radiate the power flux coming from the core. High evaporation regime on the other hand corresponds to Li radiation in the SOL as high as 150MW, which is the result of low electron temperature at the plate ($<$ 10eV) and higher Li dilution in the edge. Maximum local power to the plate value is below 5MW/m^2 and satisfies the technological limit. In both regimes core plasma conditions remain comparable. Li concentration in the core is between 13% (low evaporation) and 15% (high evaporation) for density at the separatrix $n_{sep} = 3.63 \times 10^{19}\mathrm{m}^{-3}$. Power across the separatrix is 160MW for $n_{sep} = 3.63 \times 10^{19}\mathrm{m}^{-3}$ in the case of high evapoaration regime which remains above the L-H transiton threshold.

Acknowledgements

This work has been carried out within the framework of the EUROfusion Consortium and has received funding from the Euratom research and training programme 2014-2018 under grant agreement No 633053. The views and opinions expressed herein do not necessarily reflect those of the European Commission. This scientific work was partly supported by Polish Ministry of Science and Higher Education within the framework of the scientific financial resources in the year 2018 allocated for the realization of the international co-financed project.

References

[1] V.A. Evtikhin, *et al.*, *Fusion Eng. Des.* **56-57** 363-367 (2001)
[2] R.E. Nyrgen, F.E. Tabarés, *Nuclear Materials and Energy* **9**, 6-21, (2016)
[3] Ono M. United States: Nova Scientific Publications (August 2012), 2012. Web. doi:10.2172/1056493.
[4] T.W. Morgan, *et al.*, *Nucl. Materials and Energy*, **12**, 210-215 (2017)
[5] J.W. Coenen ,*et al.* , *Phys. Scripta* **T159**, 014037, (2014)
[6] G. Mazzitelli, *et al.*, *J. Nucl. Mater.* **463**, 1152-1155 (2015)
[7] R. Zagórski, *et al.*, *Nucl. Fusion*, **53**, 073030 (2013)
[8] I. Ivanova-Stanik, *et al.*, *Contrib. Plasma Phys.* **54**, No. 4-6, 442 – 447 (2014)
[9] R. Zagórski, *et al.*, *J. Nucl. Mater.* **463**, 649–653 (2015)
[10] K. Gałązka, *et al.*, *Contrib. Plasma Phys.* **56**, No. 6-8, 772 – 777 (2016) DOI: 10.1002/ctpp.201610008
[11] R. Zagórski, *et al.*, *Fusion Eng. and Design* **122** 313-321 (2017)
[12] G. Telesca, *et al.*, *J. Nucl. Mater.* **438** (Supplement), S567 (2013)
[13] M. Poradziński, *et al.*, *Fusion Eng. and Design* **124** 248-251 (2017)
[14] V. Pericoli Ridolfini, *et al.*, *A Comparative Study of the Effects of Liquid Lithium and Tin as DEMO Divertor Targets on the Heat Loads and SOL Properties*, sent to Physics of Plasmas
[15] R. Kemp, *et al.*, EFDA Report WP11-SYS-01-ACT5 (2012).
[16] C. B. Alcock, V. P. Itkin and M. K. Horrigan, *Canadian Metallurgical Quarterly* 1984; **23**(3), 309-313. DOI: 10.1179/cmq.1984.23.3.309
[17] C. Y. Ho, R. W. Powell and P. E. Liley, *J. Phys. Chem. Ref. Data* **1**, 279 (1972). DOI: 10.1063/1.3253100
[18] Y. R. Martin, *et al.*, *Journal of Physics: Conf. Series* 123, 012033 (2008)